Microporous and Mesoporous Materials 267 (2018) 124–133

Contents lists available at ScienceDirect

Microporous and Mesoporous Materials

journal homepage: www.elsevier.com/locate/micromeso

Effect of Ge/Si substitutions on the local geometry of Si framework sites in zeolites: A combined high resolution ^{29}Si MAS NMR and DFT/MM study on zeolite Beta polymorph C (BEC)

Sarah R. Whittleton[a], Aurelie Vicente[b], Christian Fernandez[b], Somayeh F. Rastegar[a], Anna V. Fishchuk[a], Stepan Sklenak[a,*]

[a] J. Heyrovský Institute of Physical Chemistry, The Czech Academy of Sciences, Dolejškova 3, 182 23 Prague 8, Czech Republic
[b] Laboratoire Catalyse et Spectrochimie, ENSICAEN, Université de Caen, CNRS, 6 bd du Maréchal Juin, Caen, 14050, France

ARTICLE INFO

Keywords:
BEC
Zeolite Beta polymorph C
Ge-zeolites
Germanoaluminosilicates
^{29}Si MAS NMR

ABSTRACT

We employed density functional theory/molecular mechanics (DFT/MM) calculations and ^{29}Si magic-angle spinning (MAS) NMR spectroscopy to investigate the effect of single and multiple Ge/Si substitutions on the ^{29}Si NMR parameters as well as the local geometry of *Si*O_4 tetrahedra of the nearest (Ge-O-*Si*) and next-nearest (Ge-O-Si-O-*Si*) neighboring *Si* atoms. The influences of the Ge/Si substitutions are compared with the effects of the corresponding Al/Si substitutions (i.e., Al-O-*Si* and Al-O-Si-O-*Si*, respectively). Zeolite Beta polymorph C (BEC), containing double four-membered rings (D4Rs) and exhibiting three distinguishable T sites in the framework, was chosen for this study as a model of germanium containing zeolites. Our computations give a systematic downshift of the ^{29}Si chemical shift of *Si* by 1–6 ppm for Ge-O-*Si* sequences. Furthermore, the contributions of two, three, and four Ge atoms as the nearest neighbors to the downshift of *Si* are not additive and the calculated downshifts lie in the intervals from 2 to 6 ppm, from 1 to 9 ppm, and from 5 to 11 ppm, respectively. Conversely, the contributions of two, three, and four Al atoms as the nearest neighbors are approximately additive. The downshifts caused by Ge nearest neighbors are less than half compared with the corresponding downshifts caused by Al. Moreover, our calculations show that there are no systematic contributions of Ge and Al as next-nearest neighbors (i.e., Ge-O-Si-O-*Si* and Al-O-Si-O-*Si*, respectively) to the ^{29}Si chemical shift of *Si*, and not even the direction (sign) can be predicted without calculating the corresponding sequence.

1. Introduction

Zeolites are crystalline microporous aluminosilicates made of corner-sharing TO_4 tetrahedra (T = Si, Al^-). They are widely used as molecular sieves and catalysts in industrial chemical processes [1–5]. Germanium can isomorphically substitute silicon in zeolites (i.e., T = Ge). Many zeolitic structures with framework Ge atoms have been obtained (e.g., BEC [6–9], FAU [10–12], LTA [10,13], MFI [14–19], MON [20], NAT [21], RHO [22], SOD [23–26]). In addition, a large number of new zeolite topologies with pore sizes ranging from eight-membered ring to 30-membered ring, all of them containing double four-membered rings (D4Rs) as structural units, have been synthesized using Ge containing gels [27,28].

High-resolution ^{29}Si MAS NMR spectroscopy represents a powerful tool to characterize the local structures of SiO_4 in microporous aluminosilicate frameworks [29–34]. Interpretations of ^{29}Si MAS NMR experiments on various zeolites were originally based on simple linear correlation between the ^{29}Si chemical shift δ(Si) and the average T-O-T angle (θ) of the zeolite framework [35,36]. In addition, there are known ranges of the ^{29}Si chemical shift for framework Si atoms possessing a different number of Al atoms as the nearest neighbors (i.e., Si(3Si,1Al), Si(2Si,2Al), Si(1Si,3Al), and Si(0Si,4Al)) for different zeolite frameworks [37–39]. Conversely, there is no empirical correlation between the structural parameters and the corresponding ^{29}Si NMR parameters available in the literature for Si atoms with Ge atoms as the nearest neighbors. For germanosilicates and germanoaluminosilicates, there are even not known intervals of the ^{29}Si chemical shift for framework Si atoms with a different number of Ge atoms as the nearest neighbors (i.e., Si(3Si,1Ge), Si(2Si,2Ge), Si(1Si,3Ge), and Si(0Si,4Ge)).

Advances in quantum chemistry allowed calculations of NMR shielding for ^{29}Si atoms in silicate and aluminosilicate frameworks to interpret ^{29}Si MAS NMR spectra [33,34,40–46]. Recently, a QM/MM approach was successfully employed to study the effect of substitution of Si for Al on the ^{29}Si NMR parameters as well as the local geometry of

* Corresponding author.
E-mail address: stepan.sklenak@jh-inst.cas.cz (S. Sklenak).

https://doi.org/10.1016/j.micromeso.2018.03.021
Received 3 January 2018; Received in revised form 14 March 2018; Accepted 15 March 2018
Available online 16 March 2018
1387-1811/

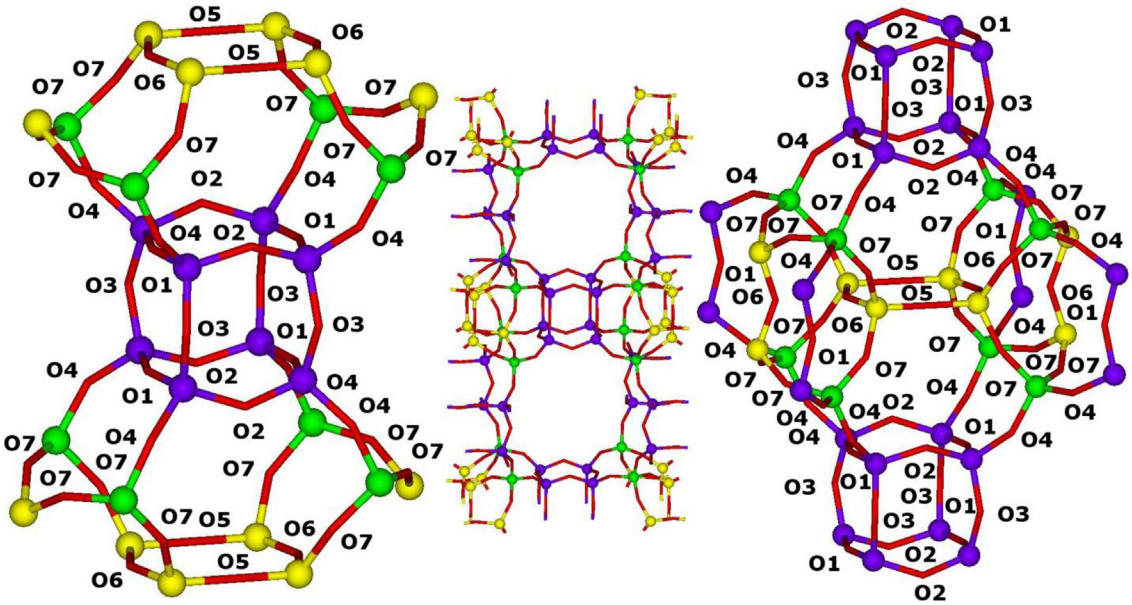

Fig. 1. Positions of the T1 (violet), T2 (green), T3 (yellow), and inequivalent oxygen (O1, O2, …O7) atoms in the BEC framework. Each T1 atom has three T1 and one T2 nearest neighbors. Each T2 atom has two T1 and two T3 nearest neighbors. Each T3 atom has two T2 and two T3 nearest neighbors. (For interpretation of the references to colour in this figure legend, the reader is referred to the Web version of this article.)

SiO_4 tetrahedra of the nearest and next-nearest neighboring Si atom in the silicon-rich zeolite of the chabazite structure [34].

In this paper, employing QM/MM calculations [34] together with the bare zeolite framework model [34,47–52] in a combination with high-resolution ^{29}Si MAS NMR experiments, we investigate the effects of one, two, three, and four framework Ge atoms as the nearest neighbors on the ^{29}Si chemical shift of *Si* (i.e., *Si*(3Si,1Ge), *Si*(2Si,2Ge), *Si*(1Si,3Ge), and *Si*(0Si,4Ge), respectively) and the local geometry of *Si*O_4 tetrahedra in frameworks of germanium containing zeolites. The calculated influences of Ge are compared with the corresponding effects of framework Al atoms. Moreover, the influences of concomitant Ge/Si and Al/Si substitutions (i.e., Si(T)(2Si,1Al,1Ge)) are studied as well. The effects of one framework Ge atom as a next-nearest (Ge-O-Si-O-*Si*) neighbor are also investigated.

Zeolite Beta polymorph C (BEC), containing double four-membered rings (D4Rs) in the framework, was chosen for this study as a model of germanium containing zeolites. There are only three crystallographically distinguishable T sites (T1, T2, and T3) in the BEC framework. This study is aimed to give guidance in interpretations of ^{29}Si MAS NMR spectra of Ge-zeolites, many of which contain D4R units, and other Ge containing (alumino)silicate matrixes.

2. Experimental section

2.1. Samples

Two samples of the BEC structure from our prior study [53] were studied by ^{29}Si MAS NMR spectroscopy: germanosilicate zeolite (BEC-Ge; Si/Ge ratio of 3.6) and germanoaluminosilicate zeolite (BEC-Ge/Al; Si/Ge and Si/Al ratios of 6.7 and 30.8, respectively). The former material containing only Si and Ge tetrahedral atoms allows the experimental investigation of the effect of Ge without the interference of framework Al atoms while the latter zeolite which additionally contains framework Al atoms is a model system of the BEC-type catalytic material. The synthesis, the alumination procedure, and the characterization of the two studied samples are described in detail in our previous study [53].

Since the BEC-Ge and BEC-Ge/Al samples contained their organic directing agent, the samples were calcined under air at 500 °C for 2 h. However, ^{29}Si MAS NMR experiments showed that the structure of the BEC-Ge sample collapsed during the calcination due to the presence of moisture while the BEC-Ge/Al sample maintained its crystallinity. Therefore, the BEC-Ge sample was carefully calcined at 500 °C under oxygen without exposure to humidity to preserve its crystallinity prior to the NMR experiments. The sample was then transferred into 4 mm-OD ZrO_2 rotors directly in a vacuum line and the rotors were closed with tightly fitting Kel-F caps.

2.2. ^{29}Si MAS NMR spectroscopy

^{29}Si Solid-state MAS NMR spectra of the BEC-Ge and BEC-Ge/Al samples were recorded on a Bruker Avance III 400 (9.4 T) spectrometer at a frequency of 79.5 MHz using a 4-mm-OD ZrO_2 rotor and a double-resonance probehead. All the MAS NMR experiments were performed using a sample spinning speed of 14 kHz and tetramethylsilane (TMS) as the chemical shift reference. Single pulse excitation with pulse lengths of 7.0 μs (30° flip angle) and 60 s recycling delay were used and 5120 and 2048 scans for the BEC-Ge and BEC-Ge/Al, respectively, samples were recorded. ^{1}H→^{29}Si cross-polarization (CP) MAS NMR experiments for the BEC-Ge/Al samples were carried out as well. The CP MAS NMR measurements were performed with a contact time of 4 ms, a recycling time of 1 s, and 51200 scans.

3. BEC-type material

Zeolite Beta (BEA) has a three dimensional network of 12-membered ring pores and it is an intergrowth of two polymorphs, A and B [54]. In addition, a polymorph C was also suggested as a hypothetical structure when the structures of polymorphs were solved in 1988 [54]. More than 10 years later, polymorph C (BEC) was prepared in the pure-germanate form (FOS-5) [6], followed by all-silica [7], and germanosilicate forms (ITQ-17) [8,9]. While polymorphs A and B are the most commonly studied and industrially employed zeolite Beta [55], BEC is of interest because of its large pore size and linear 12-membered ring channels that intersect along all three crystallographic axes [53].

The BEC structure possesses three crystallographically distinguishable T sites (T1, T2, and T3) and seven symmetrically inequivalent oxygen atoms in the framework (Fig. 1) and contains double four-

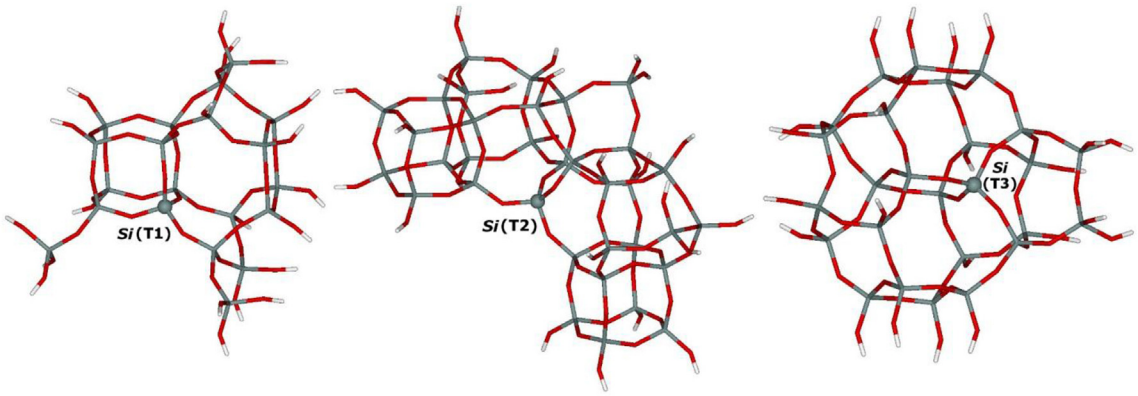

Fig. 2. Five coordination shell clusters (*Si*-O-Si-O-Si-O-H_{link}) with the center Si atom located in the T1 (left), T2 (middle), and T3 (right) sites. The *Si* atom is displayed as a ball, silicon atoms are in gray, oxygen atoms in red, and link hydrogen atoms in white. (For interpretation of the references to colour in this figure legend, the reader is referred to the Web version of this article.)

membered units (D4R) formed exclusively form the T1 atoms [56].

The stability is gained in D4R cages when germanium replaces silicon in the TO_4 tetrahedra [8] since the isomorphous substitution of Si by Ge does not introduce any framework charge but allows angles and distances to vary and thereby stabilizing such a secondary building block. Sastre et al. showed that Ge/Si substitutions into the T1 sites of BEC (i.e., into D4R units) were thermodynamically favored [57]. Similarly, Blasco et al. showed that Ge atoms selectively and preferentially occupy positions in D4R cages of the ITQ-7 [58] and ITQ-21 [59], respectively, zeolites.

Industrial application of microporous germanosilicate with a high Ge content is limited since these materials are not thermally stable and because of the high price of germanium [53]. Furthermore, since Ge atoms occupying tetrahedral sites are not charged, they cannot balance catalytically active species, that is, protons, metal cations, and metal-oxo cations. Therefore, a postsynthesis substitution of Ge for Al was developed for a BEC-type material [53]. Partial isomorphic substitution was successful, showing an increase in the Si/Ge ratio. Moreover, ^{27}Al MAS NMR experiments revealed the incorporation of tetrahedral Al into the framework [53]. Framework Al atoms stabilize the BEC zeolite framework, and furthermore, introduce a negative charge [53].

4. Computational models and methods

The QM/MM (employing the QMPOT program) approach coupled with the GIAO NMR calculations was employed to evaluate the effect of framework Ge and Al atoms as the nearest (Ge-O-*Si* and Al-O-*Si*) and next-nearest (Ge-O-Si-O-*Si* and Al-O-Si-O-*Si*) neighbors on the *Si* atom. This methodology has been shown to provide results which either reproduced observed ^{27}Al and ^{29}Si NMR parameters or permitted successful interpretations of ^{27}Al and ^{29}Si MAS NMR measurements for zeolites [34,47–50,60,61]. Therefore, we chose this approach to study the effect of framework Ge and Al atoms on the ^{29}Si chemical shift of *Si* and the local geometry of *Si*O_4 tetrahedra in frameworks of germanium containing zeolites.

4.1. QM-Pot computational model

A bare zeolite framework [34] model, which has been successfully employed in previous studies [34,47–52], that includes neither cations nor water molecules is adopted to calculate the local structure around GeO_4, AlO_4^-, and SiO_4 tetrahedra and to predict the ^{29}Si NMR shieldings. The bare charged framework was found that it represents a realistic model to describe the local geometry of AlO_4^- and SiO_4 tetrahedra and predict the ^{27}Al isotropic chemical shifts and the ^{29}Si chemical shifts in aluminosilicates [34,47–52]. Therefore, we assume that the bare framework model is appropriate to calculate the local structure of GeO_4, AlO_4^-, and SiO_4 tetrahedra and to predict the ^{29}Si NMR shieldings in germanosilicates and germanoaluminosilicates. The bare zeolite framework model is discussed in detail elsewhere [49]. The starting structure was generated from the all-silica structure solved by electron crystallography [7]. However, the numbering of the T sites has been altered to be consistent with that presented in the International Zeolite Database, see Fig. 1 [56].

QM-Pot method and programs used. The QM-Pot method employed [62,63] partitions the whole system into two parts. The inner part is treated by QM, and the outer part as well as all of the interactions between the inner and the outer layers are treated by parametrized Pot. The dangling bonds of the inner part are saturated by link hydrogen atoms. The atoms of the inner part together with the link atoms form the cluster. The QM-Pot approach is discussed in detail elsewhere [64].

The calculations were performed by the QMPOT program [63] which utilizes the Turbomole program [65–69] for the QM part and the GULP program [70,71] for the periodic potential function calculations. The DFT method employing the hybrid B3LYP [72,73] functional and the TZVP basis set of Ahlrichs et al. [74] were used for the QM calculations. Shell-model ion-pair potentials [75] parametrized on DFT results for zeolites [76] were employed as Pot. The electrostatic energy was evaluated by standard Ewald summation techniques for all cores and shells. A cutoff radius of 10 Å was chosen for the summation of short-range interactions.

QM-Pot optimization of structures. Both the lattice constants and the atomic positions of the studied systems were optimized by the force field GULP program at constant pressure. The optimized structures were subsequently used for defining a cluster around the Ge, Al, and Si atoms for the subsequent QM-Pot (DFT/force field) calculations. The clusters were embedded, and the structure of the entire system was optimized by QMPOT at constant volume.

QM-Pot cluster models. **Single centered clusters** were used to calculate the structure and the ^{29}Si NMR parameters of SiO_4 tetrahedra of a single Si atom occupying the crystallographically distinguishable T sites in the framework of all-silica BEC. The clusters have the Si atom in the center and include five coordination shells (Si-O-Si-O-Si-O-H_{link}) (Fig. 2) [34,40,47–50].

The Si atoms in the center occupied one of the distinguishable T sites of BEC. Because of the presence of silicate rings in the framework of BEC, the created clusters contained pairs of very close H_{link} atoms. Since the close H_{link} atoms represented the same Si atom, they were replaced by the corresponding $Si(OH_{link})_2$ moiety. This was repeated until the cluster contained no such pairs.

Double centered clusters were employed to evaluate the effect of one Ge and Al isomorphous substitution on the ^{29}Si chemical shift and the SiO_4 local geometry of the nearest (Ge-O-*Si*) and (Al-O-*Si*) and next-nearest (Ge-O-Si-O-*Si*) and (Al-O-Si-O-*Si*) *Si* atoms. The clusters were

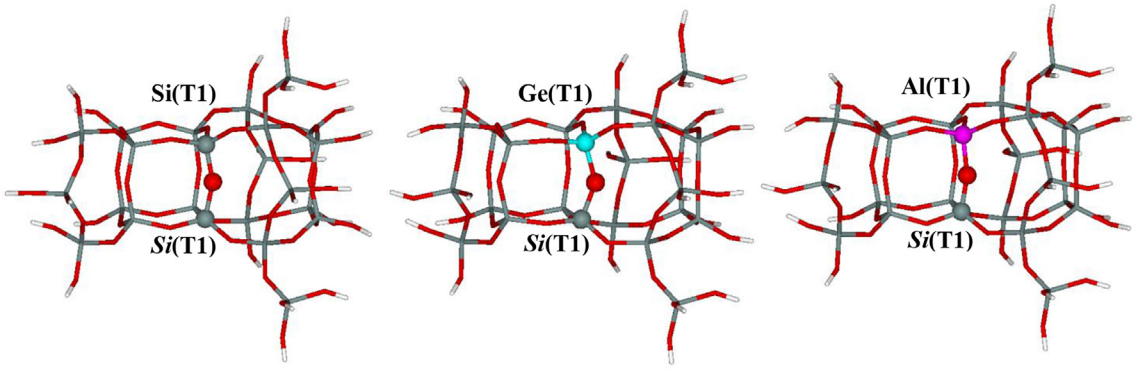

Fig. 3. Examples of double-centered clusters, centered around T site *Si*(T1) and the nearest neighbor (T1 atom) for Si-O-*Si* (left), Ge-O-*Si* (middle), and Al-O-*Si* (right), with the atoms corresponding to these sequences displayed in balls. Silicon atoms are in gray, aluminum atoms in violet, germanium atoms in blue, oxygen atoms in red, and link hydrogen atoms in white. (For interpretation of the references to colour in this figure legend, the reader is referred to the Web version of this article.)

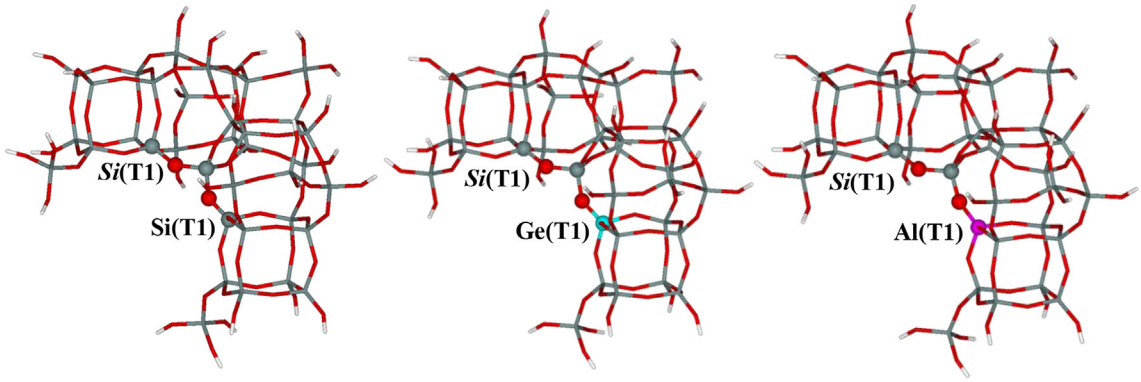

Fig. 4. Examples of double-centered clusters, centered around *Si*(T1) and the next-nearest neighbor (T1 atom) for Si-O-Si-O-*Si* (left), Ge-O-Si-O-*Si* (middle), and Al-O-Si-O-*Si* (right), with the atoms corresponding to these sequences displayed in balls. Silicon atoms are in gray, aluminum atoms in violet, germanium atoms in blue, oxygen atoms in red, and link hydrogen atoms in white. (For interpretation of the references to colour in this figure legend, the reader is referred to the Web version of this article.)

prepared by merging two five coordination shell clusters (T-O-*Si*-O-Si-O-H_{link} and *Si*-O-T-O-Si-O-H_{link} for T-O-*Si*; T-O-Si-O-*Si*-O-H_{link} and *Si*-O-Si-O-T-O-H_{link} for T-O-Si-O-*Si*), which were centered around the T (T = Ge and Al) and *Si* atoms (Figs. 3 and 4).

The calculations were carried out for three variants of the cluster for each T-O-*Si* and T-O-Si-O-*Si* sequence (T = Ge and Al). The first variant contains both the Ge and the *Si* atoms (Ge-O-*Si* and Ge-O-Si-O-*Si*), the second variant contains both the Al and the *Si* atoms (Al-O-*Si* and Al-O-Si-O-*Si*), and in the third variant the T (T = Ge and Al) atom is replaced by Si (Si-O-*Si* and Si-O-Si-O-*Si*). Using the three variants of each cluster allows comparison between the effects of Ge and Al as the nearest (T-O-*Si*) and next-nearest (T-O-Si-O-*Si*) neighbors on *Si*.

Triple, quadruple, and pentuple centered clusters were used in the same manner as the double centered clusters to calculate the effects of two, three, and four, respectively, Ge atoms as the nearest neighbors (i.e., *Si*(2Si,2Ge), *Si*(1Si,3Ge), and *Si*(0Si,4Ge), respectively). The clusters were prepared by merging three (*Si*(2Si,2Ge)), four (*Si*(1Si,3Ge)), and five (*Si*(0Si,4Ge)) five coordination shell clusters, which were centered around the Ge and *Si* atoms (Fig. 5).

Three variants of the clusters were used: first contains both the Ge atoms and the *Si* atom, the second both the Al atoms and the *Si* atom, and in the third variant the T (T = Ge and Al) atoms are replaced by Si to allow the evaluation of the effects of the Ge and Al atoms.

Furthermore, we employed in the same manner mixed Ge and Al containing triple (for *Si*(T1), *Si*(T2), and *Si*(T3)) and quadruple (only for *Si*(T1)) centered clusters to investigate the concomitant effects of both Ge and Al in Ge-O-*Si*-O-Al and $(Ge\text{-}O)_2$-*Si*(T1)-O-Al sequences in germanoaluminosilicates. The latter sequences were calculated only for *Si*(T1) to limit the number of possible combinations. The T1 framework distinguishable site was chosen because Ge/Si substitutions into the T1 sites of BEC are thermodynamically favored [57] and each Ge(T1) atom has three Si(T1) nearest neighbors.

4.2. Calculation of ^{29}Si NMR shielding

Subsequent to the QM-Pot structure determination, the GIAO NMR method [77] in the Gaussian program [78] was employed to calculate NMR shielding tensors for the *Si* atoms of the optimized clusters using the B3LYP functional. The pcS basis sets of Jensen [79] were employed, with pcS-4 for the *Si* atom of interest and pcS-1 for all the other atoms (TZVP for Ge atoms since the corresponding pcS basis sets are not available).

5. Experimental results

The ^{29}Si MAS NMR spectra of the BEC-Ge and BEC-Ge/Al samples (Fig. 6) show very broad resonances due to the presence of various different sites with close chemical shifts.

The ^{29}Si NMR resonances corresponding to Si of silanol groups (Si-OH) can overlap with those of Si in Si-O-Al sequences [34]. The CP MAS NMR experiments carried out on the BEC-Ge/Al sample indicate that the signals from ca −95 ppm to about −100 ppm correspond to Si (3Si,OH) atoms. We assume that new defects (i.e., silanol “nests”) were created during the substitution of Ge for Al in addition to the terminal silanol groups already present in the initial material.

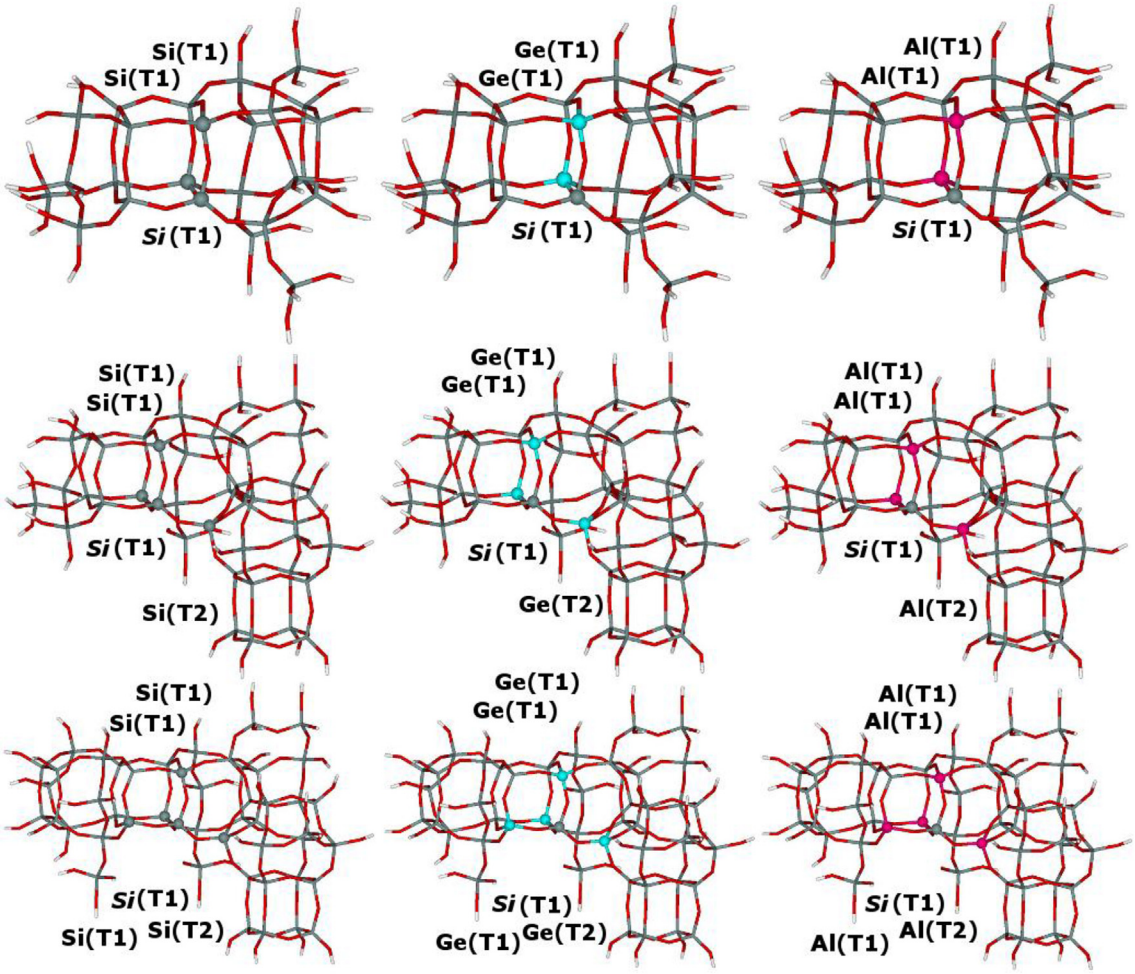

Fig. 5. Examples of triple-centered clusters, centered around T site *Si*(T1) and the two nearest Si (left, top), Ge (middle, top), and Al (right, top) neighbors (T1 atoms); quadruple-centered clusters, centered around T site *Si*(T1) and the three Si (left, middle), Ge (middle, middle), and Al (right, middle) nearest neighbors (T1 and T2 atoms); pentuple-centered clusters, centered around T site *Si*(T1) and the four Si (left, bottom), Ge (middle, bottom), and Al (right, bottom) nearest neighbors (T1 and T2 atoms). The *Si*(T1) atom and the corresponding Si, Ge, and Al nearest neighbors are displayed in balls. Silicon atoms are in gray, aluminum atoms in violet, germanium atoms in blue, oxygen atoms in red, and link hydrogen atoms in white. (For interpretation of the references to colour in this figure legend, the reader is referred to the Web version of this article.)

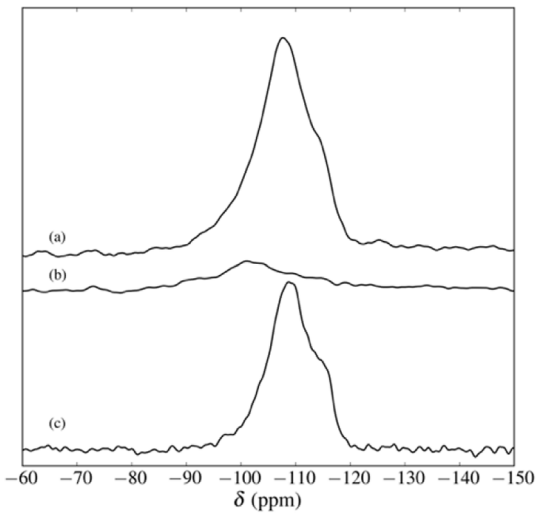

Fig. 6. ^{29}Si MAS NMR spectra of (a) BEC-Ge/Al calcined sample, (b) CP ^{1}H→^{29}Si MAS NMR spectra of BEC-Ge/Al calcined sample, (c) BEC-Ge calcined sample.

6. Computational results

6.1. Structure of SiO_4 tetrahedra and ^{29}Si chemical shifts of a single Si atom occupying the T1, T2, and T3 sites

The QM-Pot calculations using single centered clusters show three distinguishable T sites: T1, T2, and T3 which have multiplicities of 16, 8, and 8, respectively, and yield the ^{29}Si NMR shieldings and the average T-O-T angles of the three distinguishable T sites of the BEC framework (Table 1).

A chabazite sample having a Si/Al ratio of 38 was employed to convert the calculated ^{29}Si NMR shieldings into the ^{29}Si chemical shifts (Table 1) [34,49]. Table 1 also reports the three distinct experimental ^{29}Si chemical shifts for the all-silica BEC obtained by Corma et al. [80] (i.e., −110, −112, and −116 ppm), which can be assigned to the T sites using the calculations in this study. The calculated ^{29}Si chemical shifts (Table 1) are plotted against the average T-O-T angles for the three T sites in Fig. S1 of the Supplementary material.

6.2. Effect of one Ge/Si and Al/Si substitution on the nearest Si atom (Ge-O-Si) and (Al-O-Si)

Single Ge/Si and Al/Si substitutions are performed for all four

Table 1
^{29}Si NMR shieldings in ppm, average T-O-T angles in deg, and ^{29}Si chemical shifts in ppm of *Si* in the distinguishable T sites (T1, T2, and T3) of the BEC framework.

T site	Multiplicity	^{29}Si NMR shielding	Average T-O-T angle	^{29}Si chemical shift	
				Calculated[a]	Observed[b]
Si(T1)	16	449.4	148.5	−110.7	−110
Si(T2)	8	449.8	148.7	−111.1	−112
Si(T3)	8	455.7	154.7	−117.0	−116

[a] The ^{29}Si chemical shifts were obtained by a conversion of the GIAO NMR shieldings using the calculated and measured shielding/shift values of 450.2 ppm and −111.5 ppm, respectively, for the chabazite sample [34,49]. The multiplicity of the three T sites (2:1:1 for T1:T2:T3) of BEC is taken into account as well [56].
[b] The observed ^{29}Si chemical shift are taken from Ref. [80].

nearest TO_4 neighbors of each of the three crystallographically distinguishable T sites (T1, T2, and T3) in the BEC framework (see Fig. 3). The ^{29}Si NMR shieldings, the ^{29}Si chemical shifts, and the average T-O-T angles of the SiO_4 of the optimized structures are reported in Table S1 of the Supplementary material. The ^{29}Si chemical shifts are also listed in Tables 2 and 3. Furthermore, the ^{29}Si chemical shifts are plotted against the average T-O-T angles in Fig. S2 of the Supplementary material. The figure reveals good correlation especially for Ge.

Table S1 of the Supplementary material compares the Ge- and Al-substituted sequences (Ge-O-*Si* and Al-O-*Si*) to the non-substituted (Si-O-*Si*) all-silica framework to reveal the effects of these isomorphous substitutions. For all three T sites, the calculations for Ge-O-*Si* sequences yield a systematic downshift (Δ) of the ^{29}Si chemical shift of *Si* by 1.3–6.0 ppm as well as mainly a decrease in the average T-O-T angle by −0.3–4.6°. It should be noted that the magnitude of the effect of Ge substitution is generally the smallest for *Si* in the T3 site. Table S1 of the Supplementary material reveals that for the Al-O-*Si* sequences there is a systematic downshift (Δ) of ^{29}Si chemical shift of *Si* by 3.2–10.8 ppm as well as mainly a decrease in the average T-O-T angle by −0.4–4.4°, respectively.

6.3. Effects of two Ge/Si and Al/Si substitutions on the nearest Si(2Si,2Ge) and Si(2Si,2Al) atoms, respectively

Two Ge/Si and Al/Si substitutions are made for all four nearest TO_4 neighbors of each of the three crystallographically distinguishable T sites (T1, T2, and T3) in the BEC framework (see Fig. 5). The ^{29}Si NMR shieldings, the ^{29}Si chemical shifts, and the average T-O-T angles of the SiO_4 of the optimized structures are listed in Table S2 of the Supplementary material. The ^{29}Si chemical shifts are also listed in Tables 2 and 3. Moreover, the ^{29}Si chemical shifts are plotted against the average T-O-T angles in Fig. S3 of the Supplementary material. The figure reveals good correlation particularly for Ge.

Table S2 of the Supplementary material compares the effects of two Ge and Al atoms as the nearest neighbors (i.e., *Si*(2Si,2Ge) and *Si*(2Si,2Al)) to the non-substituted all silica framework. The calculated downshifts (Δ) of *Si* caused by two Ge and Al lie in the range from 1.6 to 6.3 ppm and from 6.5 to 18.1 ppm, respectively. The calculations reveal that the contributions of the two Ge atoms as the nearest neighbors to the downshift of *Si* are not additive (i.e., $\Delta \neq \Sigma$; Σ is the sum of the two individual downshifts (Table S1 of the Supplementary material) of the corresponding Ge atoms) in most cases while the contributions of two Al atoms are approximately additive (i.e., $\Delta \approx \Sigma$; Σ is the sum of the two individual downshifts (Table S1 of the Supplementary material) of the corresponding Al atoms). Table S2 of the Supplementary material also shows mainly a decrease in the average T-O-T angle by −1.2–4.4° (Ge) and −4.3–7.5° (Al).

6.4. Effects of three Ge/Si and Al/Si substitutions on the nearest Si (1Si,3Ge) and Si(1Si,3Al) atoms, respectively

Three Ge/Si and Al/Si substitutions are carried out for all four nearest TO_4 neighbors of each of the three crystallographically distinguishable T sites (T1, T2, and T3) in the BEC framework (see Fig. 5). The ^{29}Si NMR shieldings, the ^{29}Si chemical shifts, and the average T-O-T angles of the SiO_4 of the optimized structures are shown in Table S3 of the Supplementary material The ^{29}Si chemical shifts are also listed in Tables 2 and 3. In addition, the ^{29}Si chemical shifts are plotted against the average T-O-T angles in Fig. S4 of the Supplementary material. The figure reveals excellent correlation for both Ge and Al.

Similarly, as for two Ge and Al nearest neighbors, Table S3 of the Supplementary material shows that three Ge/Si and Al/Si substitutions cause a downshift (Δ) of *Si*(2Si,2Ge) and *Si*(2Si,2Al), respectively, from 0.6 to 8.9 ppm and from 13.6 to 23.2 ppm, respectively. Table S3 of the Supplementary material reveals that the contributions of the three Ge atoms as the nearest neighbors to the downshift of *Si* are not additive (i.e., $\Delta \neq \Sigma$; Σ is the sum of the three individual downshifts (Table S1 of the Supplementary material) of the corresponding Ge atoms) while the

Table 2
^{29}Si chemical shifts (in ppm) of Si(T)(4Si,0Ge), Si(T)(3Si,1Ge), Si(T)(2Si,2Ge), Si(T)(1Si,3Ge), and Si(T)(0Si,4Ge) atoms for T = T1, T2, and T3.

nearest neighbors	δ(*Si*(T1))[a]	nearest neighbors	δ(*Si*(T2))[a]	nearest neighbors	δ(*Si*(T3))[a]
	−110.0		−112.0		−116.0
Ge(T1)[b]	−104.0	Ge(T1)	−108.3	Ge(T2)	−114.5
Ge(T1)[b]	−107.7	Ge(T3)	−108.9	Ge(T3)[c]	−114.7
Ge(T1)[b]	−107.6			Ge(T3)[c]	−114.3
Ge(T2)	−106.7				
Ge(T1), Ge(T1)[d]	−104.3	Ge(T1), Ge(T1)	−107.6	Ge(T2), Ge(T2)	−114.1
Ge(T1), Ge(T1)[d]	−108.4	Ge(T1), Ge(T3)	−105.7	Ge(T2), Ge(T3)[e]	−111.9
Ge(T1), Ge(T1)[d]	−105.8	Ge(T3), Ge(T3)	−106.6	Ge(T2), Ge(T3)[e]	−113.3
Ge(T1), Ge(T2)[f]	−104.7			Ge(T3), Ge(T3)	−112.5
Ge(T1), Ge(T2)[f]	−103.7				
Ge(T1), Ge(T2)[f]	−107.2				
Ge(T1), Ge(T1), Ge(T1)	−107.0	Ge(T1), Ge(T1), Ge(T3)	−104.6	Ge(T2), Ge(T2), Ge(T3)[g]	−111.5
Ge(T1), Ge(T1), Ge(T2)[h]	−104.6	Ge(T1), Ge(T3), Ge(T3)	−103.1	Ge(T2), Ge(T2), Ge(T3)[g]	−115.4
Ge(T1), Ge(T1), Ge(T2)[h]	−106.9			Ge(T2), Ge(T3), Ge(T3)	−109.4
Ge(T1), Ge(T1), Ge(T2)[h]	−104.7				
Ge(T1), Ge(T1), Ge(T1), Ge(T2)	−105.3	Ge(T1), Ge(T1), Ge(T3), Ge(T3)	−101.0	Ge(T2), Ge(T2), Ge(T3), Ge(T3)	−111.0

[a] The ^{29}Si chemical shifts in ppm were obtained as follows: δ(Si(T1)) = −110.0 + Δ(shieldings) for Si in T1; δ(Si(T2)) = −112.0 + Δ(shieldings) for Si in T2; δ(Si(T3)) = −116.0 + Δ(shieldings) for Si in T3; where −110.0, −112.0, −116.0 are the experimental ^{29}Si chemical shifts [80] in ppm assigned to Si in T1, T2, and T3, respectively.
[b, c, d, e, f, g, h] The corresponding clusters have symmetrically inequivalent O atoms.

Table 3
^{29}Si chemical shifts (in ppm) of Si(T)(4Si,0Al), Si(T)(3Si,1Al), Si(T)(2Si,2Al), Si(T)(1Si,3Al), and Si(T)(0Si,4Al) atoms for T = T1, T2, and T3.

nearest neighbors	δ(*Si*(T1))[a]	nearest neighbors	δ(*Si*(T2))[a]	nearest neighbors	δ(*Si*(T3))[a]
	−110.0		−112.0		−116.0
Al(T1)[b]	−101.7	Al(T1)	−106.1	Al(T2)	−110.0
Al(T1)[b]	−101.8	Al(T3)	−102.5	Al(T3)[c]	−105.2
Al(T1)[b]	−104.9			Al(T3)[c]	−108.3
Al(T2)	−106.8				
Al(T1), Al(T1)[d]	−93.3	Al(T1), Al(T1)	−103.3	Al(T2), Al(T2)	−103.8
Al(T1), Al(T1)[d]	−97.4	Al(T1), Al(T3)	−98.3	Al(T2), Al(T3)[e]	−98.0
Al(T1), Al(T1)[d]	−96.3	Al(T3), Al(T3)	−93.9	Al(T2), Al(T3)[e]	−104.3
Al(T1), Al(T2)[f]	−98.6			Al(T3), Al(T3)	−98.5
Al(T1), Al(T2)[f]	−99.2				
Al(T1), Al(T2)[f]	−103.5				
Al(T1), Al(T1), Al(T1)	−88.7	Al(T1), Al(T1), Al(T3)	−95.1	Al(T2), Al(T2), Al(T3)[g]	−94.6
Al(T1), Al(T1), Al(T2)[h]	−93.3	Al(T1), Al(T3), Al(T3)	−90.2	Al(T2), Al(T2), Al(T3)[g]	−102.4
Al(T1), Al(T1), Al(T2)[h]	−95.6			Al(T2), Al(T3), Al(T3)	−92.8
Al(T1), Al(T1), Al(T2)[h]	−95.9				
Al(T1), Al(T1), Al(T1), Al(T2)	−90.0	Al(T1), Al(T1), Al(T3), Al(T3)	−87.0	Al(T2), Al(T2), Al(T3), Al(T3)	−91.2

[a] The ^{29}Si chemical shifts in ppm were obtained as follows: δ(Si(T1)) = −110.0 + Δ(shieldings) for Si in T1; δ(Si(T2)) = −112.0 + Δ(shieldings) for Si in T2; δ(Si(T3)) = −116.0 + Δ(shieldings) for Si in T3; where −110.0, −112.0, −116.0 are the experimental ^{29}Si chemical shifts [80] in ppm assigned to Si in T1, T2, and T3, respectively.
[b, c, d, e, f, g, h] The corresponding clusters have symmetrically inequivalent O atoms.

contributions of three Al atoms are approximately additive (i.e., Δ ≈ Σ; Σ is the sum of the three individual downshifts (Table S1 of the Supplementary material) of the corresponding Al atoms). Table S3 of the Supplementary material also shows both an increase (minus sign) and a decrease (plus sign) in the average T-O-T angle by −2.6–4.4° (Ge) and −6.2–8.2° (Al).

6.5. Effects of four Ge/Si and Al/Si substitutions on the nearest Si(0Si,4Ge) and Si(0Si,4Al) atoms, respectively

Four Ge/Si and Al/Si substitutions are performed for all four nearest TO_4 neighbors of each of the three crystallographically distinguishable T sites (T1, T2, and T3) in the BEC framework (see Fig. 5). The ^{29}Si NMR shieldings, the ^{29}Si chemical shifts, and the average T-O-T angles of the *Si*O_4 of the optimized structures are revealed in Table S4 of the Supplementary material. The ^{29}Si chemical shifts are also listed in Tables 2 and 3. Furthermore, the ^{29}Si chemical shifts are plotted against the average T-O-T angles in Fig. S5 of the Supplementary material. Table S4 of the Supplementary material reveals that *Si*(0Si,4Ge) and *Si*(0i,4Al) atoms are downshifted (Δ) by 4.7–11.0 ppm and 20.0–25.0 ppm, respectively. The contributions of four Ge are non-additive (i.e., Δ ≠ Σ; Σ is the sum of the four individual downshifts (Table S1 of the Supplementary material) of the corresponding Ge atoms)) while those of four Al are approximately additive (i.e., Δ ≈ Σ; Σ is the sum of the four individual downshifts (Table S1 of the Supplementary material) of the corresponding Al atoms). The calculated average T-O-T angle is decreased by up to 5° (Ge) and 4° (Al).

6.6. Effects of mixed Ge/Si and Al/Si substitutions on the nearest Si (2Si,1Ge,1Al) and Si(T1)(Si,2Ge,1Al) atoms

One Ge/Si and one Al/Si concomitant substitutions are made for all four nearest TO_4 neighbors of each of the three crystallographically distinguishable T sites (T1, T2, and T3) in the BEC framework. Furthermore, two Ge/Si and one Al/Si concomitant substitutions are performed for all four nearest TO_4 neighbors of T1. The ^{29}Si NMR shieldings, the ^{29}Si chemical shifts, and the average T-O-T angles of the *Si*O_4 of the optimized structures are shown in Table S5 of the Supplementary material. The ^{29}Si chemical shifts of the Si(T)(2Si,1Al,1Ge) atoms are also listed in Table 4. Moreover, the ^{29}Si chemical shifts are plotted against the average T-O-T angles for the Si(T)(2Si,1Al,1Ge) atoms in Fig. S6 of the Supplementary material. The figure reveals good correlation.

Table S5 of the Supplementary material compares the effects of one Ge/Si and one Al/Si concomitant substitutions (i.e., *Si*(2Si,1Ge,1Al)) and two Ge/Si and one Al/Si concomitant substitutions (i.e., *Si*(T1)(Si,2Ge,1Al)) to the non-substituted all silica framework. The calculated downshifts (Δ) of *Si* of *Si*(2Si,1Ge,1Al) lie in the range from 2.1 to 13.4 ppm while those of *Si* of *Si*(T1)(Si,2Ge,1Al) from 3.8 to 12.3 ppm. The calculations reveal that the contributions of the one Ge and one Al as the nearest neighbors to the downshift of *Si* are approximately additive (i.e., Δ ≈ Σ; Σ is the sum of the two individual downshifts (Table S1 of the Supplementary material) of the corresponding Ge and Al atoms) in most cases while the contributions of two Ge and one Al are not additive (i.e., Δ ≠ Σ; Σ is the sum of the two individual downshifts (Table S1 of the Supplementary material) of the corresponding Ge atoms and one individual downshift of the Al atom). Table S5 of the Supplementary material also shows mainly a decrease in the average T-O-T angle by −4.5–6.8° for *Si*(2Si,1Ge,1Al) and −3.9–5.3° for *Si*(T1)(Si,2Ge,1Al).

6.7. Effect of Ge/Si and Al/Si substitutions on the next-nearest Si atom (Ge-O-Si-O-Si) and (Al-O-Si-O-Si)

16 next-nearest neighbor positions were selected for a single isomorphous substitution of Si for Al or Ge at a T site in the BEC framework. The ^{29}Si NMR shieldings, the ^{29}Si chemical shifts, and the average T-O-T angles of the *Si*O_4 of the optimized structures are reported in Table S6 of the Supplementary material. In addition, the ^{29}Si chemical shifts are plotted against the average T-O-T angles in Fig. S7 of the Supplementary material. The figure reveals good correlation for both Ge and Al.

Table S6 of the Supplementary material compares the Ge- and Al-substituted structures (Ge-O-Si-O-*Si* and Al-O-Si-O-*Si*) to the non-substituted (Si-O-Si-O-*Si*) all-silica framework to reveal the effects of this isomorphous substitution. The findings in Table S6 of the Supplementary material regarding the effects of the substitution (Δ values) on the ^{29}Si NMR shielding vary depending on the T site and the atom that is substituted (Ge or Al). The Δ values for the ^{29}Si NMR shielding values range from −2.6–2.2 ppm for Ge and −2.1–3.3 ppm for Al. However, the majority of the Δ values for Ge and Al are less than ± 1.0 and ± 2.0 ppm, respectively. The largest Δ values in shielding are observed at the T3 site, specifically when substitution occurs at a T3 next-nearest neighbor (upshift −2.6 ppm). In addition, an Al next-nearest neighbor substitution has a larger effect on shielding than the respective Ge next-nearest neighbor.

Table 4
^{29}Si chemical shifts (in ppm) of Si(T)(2Si,1Al,1Ge) atoms for T = T1, T2, and T3.

nearest neighbors	$\delta(Si(T1))^a$	nearest neighbors	$\delta(Si(T2))^a$	nearest neighbors	$\delta(Si(T3))^a$
Al(T1), Ge(T1)[b]	−97.7	Al(T1), Ge(T1)	−105.0	Al(T2), Ge(T2)	−108.7
Al(T1), Ge(T1)[b]	−98.3	Al(T1), Ge(T3)	−103.9	Al(T2), Ge(T3)[c]	−102.6
Al(T1), Ge(T1)[b]	−102.2	Ge(T1), Al(T3)	−99.1	Al(T2), Ge(T3)[c]	−107.7
Al(T1), Ge(T1)[b]	−103.6	Al(T3), Ge(T3)	−100.1	Ge(T2), Al(T3)[d]	−106.0
Al(T1), Ge(T1)[b]	−101.3			Ge(T2), Al(T3)[d]	−108.4
Al(T1), Ge(T1)[b]	−102.2			Al(T3), Ge(T3)[e]	−103.3
Al(T1), Ge(T2)[f]	−98.4			Al(T3), Ge(T3)[e]	−107.5
Al(T1), Ge(T2)[f]	−97.5				
Al(T1), Ge(T2)[f]	−102.5				
Ge(T1), Al(T2)[g]	−104.3				
Ge(T1), Al(T2)[g]	−103.5				
Ge(T1), Al(T2)[g]	−107.9				

[a] The ^{29}Si chemical shifts in ppm were obtained as follows: δ(Si(T)) = −110.0 + Δ(shieldings) for Si in T1; δ(Si(T2)) = −112.0 + Δ(shieldings) for Si in T2; δ(Si(T3)) = −116.0 + Δ(shieldings) for Si in T3; where −110.0, −112.0, −116.0 are the experimental ^{29}Si chemical shifts [80] in ppm assigned to Si in T1, T2, and T3, respectively.
[b, c, d, e, f, g] The corresponding clusters have symmetrically inequivalent O atoms.

The effect of isomorphous substitution on the average T-O-T angle of SiO_4 is also varied, with the Δ values ranging from −2.4–3.4° for Ge and −4.3–4.0° for Al. Consistent with trends in the NMR shielding, most of the average T-O-T angles change by less than ± 1.0°, with the largest Δ values correspond when a T3 next-nearest neighbor substitution occurs at a T3 site (3.4°). Again, the effects of the next-nearest neighbor substitutions on the average T-O-T angle are typically greater for an Al substitution, than its respective Ge analog.

7. Discussion

7.1. ^{29}Si chemical shift of Si in the all-silica framework

For the all-silica BEC framework, Table 1 reveals the calculated ^{29}Si NMR shieldings, the ^{29}Si chemical shifts, and the average T-O-T angles that are distinct for the three T sites, however the T1 and T2 sites are close in magnitude and have similar average T-O-T angles. The T3 site is the most shielded, with the largest negative shift and average T-O-T angle. This is consistent with the previously observed experimental work which reports three very narrow resonances at −110, −112, and −116 ppm in the ^{29}Si MAS NMR spectra that correspond to the three crystallographically distinguishable positions of the all-silica BEC [80]. In that work, the integrated intensity of the peak at −110 ppm is significantly stronger compared to the other two resonances, indicating it belongs to the sixteen-fold T1 site, and not to the eight-fold T2 and T3 sites. This assignment also matches the calculated ^{29}Si NMR shielding values since the smallest one is calculated for *Si* in T1. The corresponding calculated ^{29}Si chemical shift of −110.7 ppm is in good agreement with the experimental value of −110 ppm. The ^{29}Si NMR resonance at −112 ppm can be assigned to *Si* in T2 since the corresponding calculated ^{29}Si chemical shift is −111.1 ppm. Our calculations predict only a very small upshift by 0.4 ppm of the ^{29}Si chemical shift of *Si* in T2 with respect to the ^{29}Si chemical shift of *Si* in T1 while the experiment reveals an upshift by 2 ppm. The resonance at −116 ppm belongs to *Si* in T3 which is calculated at −117.0 ppm. The calculated upshift of the ^{29}Si chemical shift of *Si* in T3 relative to *Si* in T1 is 6.3 ppm while the observed value is 6 ppm. Comparison of the calculated and experimental ^{29}Si chemical shifts for the all-silica BEC framework (Table 1) allows the estimation of the error of the calculated ^{29}Si chemical shift which is about 1 ppm.

7.2. ^{29}Si chemical shift of Si in germanosilicate and germanoaluminosilicate frameworks

It is well known that Al atoms as the nearest neighbor (i.e., *Si*(3Si,1Al)) strongly influence the ^{29}Si chemical shift of *Si* in aluminosilicates and that the effect of more Al atoms as the nearest neighbors on the ^{29}Si chemical shift of *Si* (i.e., *Si*(2Si,2Al), *Si*(1Si,3Al), and *Si*(0Si,4Al)) is additive [29,38,81]. The *Si*(3Si,1Al) signal is downshifted by some 6 ppm, however, the downshift can be larger, reaching 9 ppm for zeolite Beta [82] and it might reach even somewhat larger values [39]. Our computations (Table S1 of the Supplementary material) show that the effect of one Al atom as the nearest neighbor (i.e., Si(3Si,1Al)) in the BEC framework is a systematic downshift from 3 to 11 ppm. These results are close to those obtained in our prior study for the silicon-rich zeolite of the chabazite structure [34]. Furthermore, Tables S2, S3, and S4 of the Supplementary material reveal that the contributions of two, three, and four Al atoms, respectively, as the nearest neighbors are approximately additive and the calculated downshifts range from 7 to 18 ppm, from 14 to 23 ppm, and from 20 to 25 ppm, respectively. These results are in general accord with the current knowledge [39].

Conversely, the effect of Ge as the nearest neighbor on the ^{29}Si chemical shift of *Si* (i.e., Si(3Si,1Ge), Si(2Si,2Ge), Si(1Si,3Ge), and Si (0Si,4Ge)) in germanosilicates is not known. Our calculations (Table S1 of the Supplementary material) reveal that one Ge atom in Ge-O-*Si* sequences (i.e., Si(3Si,1Ge)) cause a systematic downshift of the ^{29}Si chemical shift of *Si* from 1 to 6 ppm, the majority are a downshift of 2–3 ppm. These values are only about half compared to the effects of Al is Al-O-*Si*. Moreover, Tables S2, S3, and S4 of the Supplementary material reveal that the contributions of two, three, and four Ge atoms, respectively, as the nearest neighbors to the downshift of *Si* are not additive and the calculated downshifts lie in the intervals from 2 to 6 ppm, from 1 to 9 ppm, and from 5 to 11 ppm, respectively. These values are less than half compared with the corresponding downshifts caused by Al nearest neighbors.

^{29}Si MAS NMR spectra of germanoaluminosilicates are more complex since ^{29}Si chemical shifts of framework Si atoms are affected by both Ge and Al atoms as the nearest neighbors. Our calculations (Table S5 of the Supplementary material) reveal that the contributions of one Ge atom and one Al atom as the nearest neighbors to the downshift of *Si* (i.e., *Si*(2Si,1Ge,1Al)) are approximately additive while the opposite is true for *Si*(1Si,2Ge,1Al). The reason is that the contributions of more Ge atoms as the nearest neighbors are not additive. This non-additivity complicates interpretations of ^{29}Si MAS NMR spectra of germanoaluminosilicate samples with lower Si/Ge ratios.

The previous study of the influence of Al on *Si* in Al-O-Si-O-*Si* (next-nearest neighbor) in the silicon-rich zeolite of the chabazite structure revealed a systematic downshift which ranges from 0 to 2 ppm, the majority are a downshift up to 1 ppm [34]. The results of this investigation (Table S6 of the Supplementary material) yield different results; an upshift (up to −2 ppm) for some Al-O-Si-O-*Si* sequence and a

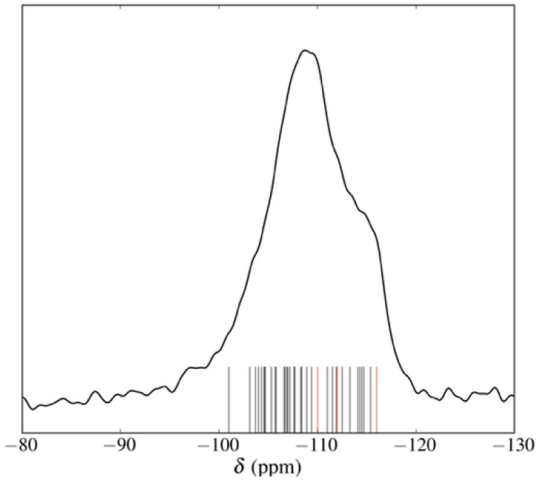

Fig. 7. ^{29}Si MAS NMR spectrum of the BEC-Ge calcined sample with the calculated ^{29}Si chemical shifts of the Si(T)(4Si,0Ge) atoms (red lines); Si(T)(3Si,1Ge), Si(T)(2Si,2Ge), Si(T)(1Si,3Ge), and Si(T)(0Si,4Ge) atoms (black lines) for T = T1, T2, and T3.

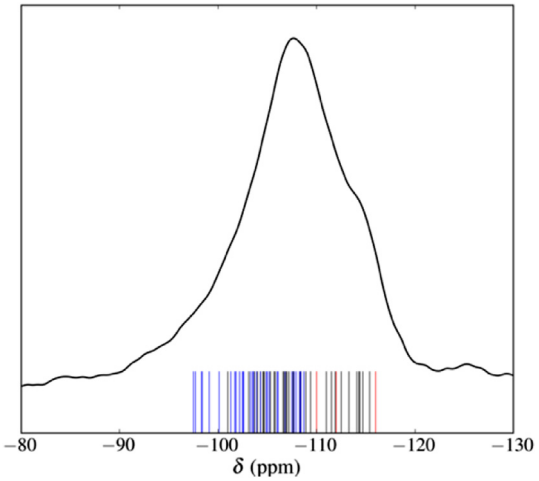

Fig. 8. ^{29}Si MAS NMR spectrum the of BEC-Ge/Al calcined sample with the calculated ^{29}Si chemical shifts of the Si(T)(4Si,0Ge,0Al) atoms (red lines); Si(T)(3Si,1Ge,0Al), Si(T)(2Si,2Ge,0Al) and Si(T)(1Si,3Ge,0Al) atoms (black lines); Si(T)(3Si,0Ge,1Al) and Si(T)(2Si,1Ge,1Al) atoms (blue lines) for T = T1, T2, and T3. (For interpretation of the references to colour in this figure legend, the reader is referred to the Web version of this article.)

downshift (up to 3 ppm) for the others. Therefore, the effect of Al on the ^{29}Si chemical shift of *Si* in Al-O-Si-O-*Si* depends on the type of the framework of the zeolite. Similarly, as for Al, our computations also reveal that Ge atoms in Ge-O-Si-O-*Si* affect the ^{29}Si chemical shift of *Si* resulting in an upshift (up to −3 ppm) for some Ge-O-Si-O-*Si* sequences and a downshift (up to 2 ppm) for the others. However, almost all of the Δ values are less than ± 1.0 ppm (Table S6 of the Supplementary material) so the effects of Ge atoms as next-nearest neighbors can be neglected for ^{29}Si MAS NMR spectra interpretations. It should be noted that for germanosilicate samples with lower Si/Ge ratios, there can be multiple Ge atoms as next-nearest neighbors and their contributions to the downshift of *Si* are not additive.

Fig. 7 compares the calculated ^{29}Si chemical shifts of Si(T)(4Si,0Ge), Si(T)(3Si,1Ge), Si(T)(2Si,2Ge), Si(T)(1Si,3Ge), and Si(T)(0Si,4Ge) atoms for T = T1, T2, and T3 (Table 2) with the observed ^{29}Si MAS NMR spectrum of the BEC-Ge calcined sample. The range of the computed ^{29}Si chemical shifts is in very good agreement with the experiment. The very low intensity ^{29}Si NMR resonance around −100 ppm belongs to surface terminal silanol groups. The ^{29}Si MAS NMR spectrum of BEC-Ge was not simulated since there are too many uncertain parameters (e.g., which of the Si(T1,2,3)(3Si,1Ge), Si(T1,2,3)(2Si,2Ge), and Si(T1,2,3)(1Si,3Ge) atoms are present in the sample, width of ^{29}Si NMR resonances, possibly the Gaussian/Lorentzian proportions of ^{29}Si NMR resonances).

Similarly, Fig. 8 compares the calculated ^{29}Si chemical shifts of Si(T)(4Si,0Ge,0Al), Si(T)(3Si,1Ge,0Al), Si(T)(3Si,0Ge,1Al), Si(T)(2Si,1Ge,1Al), Si(T)(2Si,2Ge,0Al), and Si(T)(1Si,3Ge,0Al) atoms for T = T1, T2, and T3 (Tables 2–4) with the observed ^{29}Si MAS NMR spectrum of the BEC-Ge/Al calcined sample. Both the theoretical and experimental results are in agreement. The ^{29}Si NMR resonances from around −100 ppm to ca −95 ppm correspond to silanol groups as evidenced by the CP ^{1}H→^{29}Si MAS NMR spectra. However, low intensity ^{29}Si NMR resonances of various *Si* atoms of *Si*(2Si,1Ge,1Al) can also be present in the spectrum at ca −100 ppm to −97 ppm (Table 4) and if present they would overlap with the resonances belonging to silanols. The alumination procedure increased the concentration of silanol groups in the BEC-Ge/Al sample. The ^{29}Si MAS NMR spectrum of BEC-Ge/Al was not simulated either because there are even more uncertain parameters. The good agreement between the calculated and experimental ranges of ^{29}Si chemical shifts for both the samples validates the computational approach used.

8. Conclusions

This study examines the effects of one, two, three, and four framework T (T = Ge and Al) atoms as the nearest (T-O-*Si*) neighbors on the ^{29}Si chemical shift and the SiO_4 local geometry of *Si* employing the QM-Pot approach together with the bare zeolite framework model and the GIAO NMR method. These computations give a systematic downshift of the ^{29}Si chemical shift of *Si* by 1–6 ppm and 3–11 ppm for Ge-O-*Si* and Al-O-*Si* sequences, respectively. The majority of the downshifts are 2–3 ppm for Ge and 5–8 ppm for Al. Furthermore, our results reveal that the contributions of two, three, and four Ge atoms as the nearest neighbors to the downshift of *Si* are not additive and the calculated downshifts lie in the intervals from 2 to 6 ppm, from 1 to 9 ppm, and from 5 to 11 ppm, respectively. Conversely, the contributions of two, three, and four Al atoms as the nearest neighbors are approximately additive and the calculated downshifts range from 7 to 18 ppm, from 14 to 23 ppm, and from 20 to 25 ppm, respectively. The downshifts caused by Ge nearest neighbors are less than half compared with the corresponding downshifts caused by Al.

Our calculations show that there is no systematic contribution of T (T = Ge and Al) in T-O-Si-O-*Si* sequences to the ^{29}Si chemical shift of *Si*, and not even the direction (sign) can be predicted without calculating the corresponding sequence. The effect is ± 1 and ± 2 ppm for the majority of the Ge and Al atoms, respectively.

The results of this study provide guidance in interpretations of ^{29}Si MAS NMR spectra of Ge containing zeolites and other Ge containing (alumino)silicate matrixes.

Declarations of interest

None.

Acknowledgements

This work was supported by the Grant Agency of the Czech Republic (GA 15-14007S) and the RVO 61388955. This work was supported by The Ministry of Education, Youth and Sports from the Large Infrastructures for Research, Experimental Development and Innovations project „IT4Innovations National Science Council – LM2015070“. CF and AV thank the EMC3 labex and the FEDER for the acquisition of the Avance III 400 NMR spectrometer. Financial support

from the TGIR-RMN-THC Fr3050 CNRS for conducting the research is also gratefully acknowledged. The authors acknowledge V. Valtchev (ENSICAEN) for the preparation and postsynthesis modifications of the materials studied in this work.

Appendix A. Supplementary data

Supplementary data related to this article can be found at http://dx.doi.org/10.1016/j.micromeso.2018.03.021.

References

[1] C.D. Chang, Catal. Rev. Sci. Eng. 25 (1983) 1–118.
[2] S.M. Csicsery, Pure Appl. Chem. 58 (1986) 841–856.
[3] A. Corma, A. Martinez, Catal. Rev. Sci. Eng. 35 (1993) 483–570.
[4] G. Bellussi, G. Pazzuconi, C. Perego, G. Girotti, G. Terzoni, J. Catal. 157 (1995) 227–234.
[5] J.N. Armor, Microporous Mesoporous Mater. 22 (1998) 451–456.
[6] T. Conradsson, M.S. Dadachov, X.D. Zou, Microporous Mesoporous Mater. 41 (2000) 183–191.
[7] Z. Liu, T. Ohsuna, O. Terasaki, M.A. Camblor, M.J. Diaz-Cabanas, K. Hiraga, J. Am. Chem. Soc. 123 (2001) 5370–5371.
[8] A. Corma, M.T. Navarro, F. Rey, J. Rius, S. Valencia, Angew. Chem. Int. Ed. 40 (2001) 2277–2280.
[9] A. Corma, M.T. Navarro, F. Rey, S. Valencia, Chem. Commun. (2001) 1486–1487.
[10] R.M. Barrer, J.W. Baynham, F.W. Bultitude, W.M. Meier, J. Chem. Soc. (1959) 195–208.
[11] L. Lerot, G. Poncelet, M.L. Dubru, J.J. Fripiat, J. Catal. 37 (1975) 396–409.
[12] G.M. Johnson, Y.J. Lee, A. Tripathi, J.B. Parise, Microporous Mesoporous Mater. 31 (1999) 195–204.
[13] A. Corma, F. Rey, J. Rius, M.J. Sabater, S. Valencia, Nature 431 (2004) 287–290.
[14] Z. Gabelica, J.L. Guth, Angew. Chem. Int. Ed. 28 (1989) 81–83.
[15] M.H. Tuilier, A. Lopez, J.L. Guth, H. Kessler, Zeolites 11 (1991) 662–665.
[16] H. Kosslick, V.A. Tuan, R. Fricke, C. Peuker, W. Pilz, W. Storek, J. Phys. Chem. 97 (1993) 5678–5684.
[17] L.G.A. van de Water, J.C. van der Waal, J.C. Jansen, M. Cadoni, L. Marchese, T. Maschmeyer, J. Phys. Chem. B 107 (2003) 10423–10430.
[18] A. Ghosh, N.G. Vargas, S.F. Mitchell, S. Stevenson, D.F. Shantz, J. Phys. Chem. C 113 (2009) 12252–12259.
[19] N.G. Vargas, S. Stevenson, D.F. Shantz, Microporous Mesoporous Mater. 170 (2013) 131–140.
[20] A. Tripathi, J.B. Parise, Microporous Mesoporous Mater. 52 (2002) 65–78.
[21] A. Tripathi, G.M. Johnson, S.J. Kim, J.B. Parise, J. Mater. Chem. 10 (2000) 451–455.
[22] G.M. Johnson, A. Tripathi, J.B. Parise, Microporous Mesoporous Mater. 28 (1999) 139–154.
[23] M. Wiebcke, P. Sieger, J. Felsche, G. Engelhardt, P. Behrens, J. Schefer, Z. Anorg. Allg. Chem. 619 (1993) 1321–1329.
[24] S.E. Dann, M.T. Weller, B.D. Rainford, D.T. Adroja, Inorg. Chem. 36 (1997) 5278–5283.
[25] X.H. Bu, P.Y. Feng, T.E. Gier, D.Y. Zhao, G.D. Stucky, J. Am. Chem. Soc. 120 (1998) 13389–13397.
[26] G.M. Johnson, P.J. Mead, M.T. Weller, Microporous Mesoporous Mater. 38 (2000) 445–460.
[27] G. Sastre, A. Corma, J. Phys. Chem. C 114 (2010) 1667–1673.
[28] M. Moliner, F. Rey, A. Corma, Angew. Chem. Int. Ed. 52 (2013) 13880–13889.
[29] C.A. Fyfe, G.C. Gobbi, G.J. Kennedy, J. Phys. Chem. 88 (1984) 3248–3253.
[30] J. Klinowski, C.A. Fyfe, G.C. Gobbi, J. Chem. Soc. Faraday Trans. I 81 (1985) 3003–3019.
[31] C.A. Fyfe, H. Strobl, G.T. Kokotailo, G.J. Kennedy, G.E. Barlow, J. Am. Chem. Soc. 110 (1988) 3373–3380.
[32] H. Gies, B. Marler, C. Fyfe, G. Kokotailo, Y. Feng, D.E. Cox, J. Phys. Chem. Solid. 52 (1991) 1235–1241.
[33] D.H. Brouwer, G.D. Enright, J. Am. Chem. Soc. 130 (2008) 3095–3105.
[34] J. Dedecek, S. Sklenak, C.B. Li, F. Gao, J. Brus, Q.J. Zhu, T. Tatsumi, J. Phys. Chem. C 113 (2009) 14454–14466.
[35] J.M. Thomas, J. Klinowski, S. Ramdas, B.K. Hunter, D.T.B. Tennakoon, Chem. Phys. Lett. 102 (1983) 158–162.
[36] G. Engelhardt, R. Radeglia, Chem. Phys. Lett. 108 (1984) 271–274.
[37] E. Lippmaa, M. Magi, A. Samoson, M. Tarmak, G. Engelhardt, J. Am. Chem. Soc. 103 (1981) 4992–4996.
[38] G. Engelhardt, U. Lohse, E. Lippmaa, M. Tarmak, M. Magi, Z. Anorg. Allg. Chem. 482 (1981) 49–64.
[39] K.J.D. MacKenzie, M.E. Smith, Multinuclear Solid-state NMR of Inorganic Solids, Oxford, U.K, Pergamon, 2002.
[40] B. Bussemer, K.P. Schroder, J. Sauer, Solid State Nucl. Magn. Reson. 9 (1997) 155–164.
[41] G. Valerio, A. Goursot, R. Vetrivel, O. Malkina, V. Malkin, D.R. Salahub, J. Am. Chem. Soc. 120 (1998) 11426–11431.
[42] L.M. Bull, B. Bussemer, T. Anupold, A. Reinhold, A. Samoson, J. Sauer, A.K. Cheetham, R. Dupree, J. Am. Chem. Soc. 122 (2000) 4948–4958.
[43] A. Pedone, M. Pavone, M.C. Menziani, V. Barone, J. Chem. Theor. Comput. 4 (2008) 2130–2140.
[44] D.H. Brouwer, J. Am. Chem. Soc. 130 (2008) 6306–6307.
[45] F. Dogan, K.D. Hammond, G.A. Tompsett, H. Huo, W.C. Conner, S.M. Auerbach, C.P. Grey, J. Am. Chem. Soc. 131 (2009) 11062–11079.
[46] D.H. Brouwer, I.L. Moudrakovski, R.J. Darton, R.E. Morris, Magn. Reson. Chem. 48 (2010) S113–S121.
[47] S. Sklenak, J. Dedecek, C.B. Li, B. Wichterlova, V. Gabova, M. Sierka, J. Sauer, Angew. Chem. Int. Ed. 46 (2007) 7286–7289.
[48] S. Sklenak, J. Dedecek, C.B. Li, F. Gao, B. Jansang, B. Boekfa, B. Wichterlova, J. Sauer, Collect. Czech Chem. Commun. 73 (2008) 909–920.
[49] S. Sklenak, J. Dedecek, C. Li, B. Wichterlova, V. Gabova, M. Sierka, J. Sauer, Phys. Chem. Chem. Phys. 11 (2009) 1237–1247.
[50] J. Dedecek, S. Sklenak, C. Li, B. Wichterlova, V. Gabova, J. Brus, M. Sierka, J. Sauer, J. Phys. Chem. C 113 (2009) 1447–1458.
[51] J. Dedecek, M.J. Lucero, C.B. Li, F. Gao, P. Klein, M. Urbanova, Z. Tvaruzkova, P. Sazama, S. Sklenak, J. Phys. Chem. C 115 (2011) 11056–11064.
[52] A. Vjunov, J.L. Fulton, T. Huthwelker, S. Pin, D. Mei, G.K. Schenter, N. Govind, D.M. Camaioni, J.Z. Hu, J.A. Lercher, J. Am. Chem. Soc. 136 (2014) 8296–8306.
[53] F.F. Gao, M. Jaber, K. Bozhilov, A. Vicente, C. Fernandez, V. Valtchev, J. Am. Chem. Soc. 131 (2009) 16580–16586.
[54] J.M. Newsam, M.M.J. Treacy, W.T. Koetsier, C.B. Degruyter, Proc. R. Soc. London, Ser. A 420 (1988) 375–405.
[55] C. Martinez, A. Corma, Coord. Chem. Rev. 255 (2011) 1558–1580.
[56] http://www.iza-structure.org/databases.
[57] G. Sastre, J.A. Vidal-Moya, T. Blasco, J. Rius, J.L. Jorda, M.T. Navarro, F. Rey, A. Corma, Angew. Chem. Int. Ed. 41 (2002) 4722–4726.
[58] T. Blasco, A. Corma, M.J. Diaz-Cabanas, F. Rey, J.A. Vidal-Moya, C.M. Zicovich-Wilson, J. Phys. Chem. B 106 (2002) 2634–2642.
[59] T. Blasco, A. Corma, M.J. Diaz-Cabanas, F. Rey, J. Rius, G. Sastre, J.A. Vidal-Moya, J. Am. Chem. Soc. 126 (2004) 13414–13423.
[60] J. Brus, L. Kobera, W. Schoefberger, M. Urbanova, P. Klein, P. Sazama, E. Tabor, S. Sklenak, A.V. Fishchuk, J. Dedecek, Angew. Chem. Int. Ed. 54 (2015) 541–545.
[61] P. Klein, V. Pashkova, H.M. Thomas, S.R. Whittleton, J. Brus, L. Kobera, J. Dedecek, S. Sklenak, J. Phys. Chem. C 120 (2016) 14216–14225.
[62] U. Eichler, C.M. Kolmel, J. Sauer, J. Comput. Chem. 18 (1997) 463–477.
[63] M. Sierka, J. Sauer, J. Chem. Phys. 112 (2000) 6983–6996.
[64] M. Brandle, J. Sauer, J. Am. Chem. Soc. 120 (1998) 1556–1570.
[65] M. Haser, R. Ahlrichs, J. Comput. Chem. 10 (1989) 104–111.
[66] O. Treutler, R. Ahlrichs, J. Chem. Phys. 102 (1995) 346–354.
[67] K. Eichkorn, O. Treutler, H. Ohm, M. Haser, R. Ahlrichs, Chem. Phys. Lett. 242 (1995) 652–660.
[68] K. Eichkorn, O. Treutler, H. Ohm, M. Haser, R. Ahlrichs, Chem. Phys. Lett. 240 (1995) 283–289.
[69] K. Eichkorn, F. Weigend, O. Treutler, R. Ahlrichs, Theor. Chem. Acc 97 (1997) 119–124.
[70] J.D. Gale, J. Chem. Soc., Faraday Trans. 93 (1997) 629–637.
[71] J.D. Gale, A.L. Rohl, Mol. Simulat. 29 (2003) 291–341.
[72] C.T. Lee, W.T. Yang, R.G. Parr, Phys. Rev. B 37 (1988) 785–789.
[73] A.D. Becke, J. Chem. Phys. 98 (1993) 5648–5652.
[74] A. Schafer, C. Huber, R. Ahlrichs, J. Chem. Phys. 100 (1994) 5829–5835.
[75] C.R.A. Catlow, M. Dixon, W.C. Mackrodt, Lect. Notes Phys. 166 (1982) 130–161.
[76] M. Sierka, J. Sauer, Faraday Discuss 106 (1997) 41–62.
[77] K. Wolinski, J.F. Hinton, P. Pulay, J. Am. Chem. Soc. 112 (1990) 8251–8260.
[78] M.J. Frisch, et al., Gaussian 09, Revision C.01, Gaussian, Inc., Wallingford CT, 2011.
[79] F. Jensen, J. Chem. Theor. Comput. 4 (2008) 719–727.
[80] A. Cantin, A. Corma, M.J. Diaz-Cabanas, J.L. Jorda, M. Moliner, F. Rey, Angew. Chem. Int. Ed. 45 (2006) 8013–8015.
[81] J.M. Thomas, J. Klinowski, Adv. Catal. 33 (1985) 199–374.
[82] G.H. Kuehl, H.K.C. Timken, Microporous Mesoporous Mater. 35–6 (2000) 521–532.